Electronic Supplementary Material (ESI) for CrystEngComm.
This journal is © The Royal Society of Chemistry 2022

# Supplementary Information

# One-step fabrication of nitrogen-doped laser-induced graphene derived from melamine/polyimide for enhanced flexible supercapacitors

Shuai Han,[ab‡] Cui Liu,[a‡] Nian Li,*[a] Shudong Zhang,[a] Yanping Song,[ab] Liqing Chen,[ab] Min Xi,[a] Xinling Yu,[a] Wenbo Wang,[ab] Mingguang Kong,[a] and Zhenyang Wang*[a]

[a] *Institute of Solid State Physics, CAS Key Laboratory of Photovoltaic and Energy Conservation Materials, Hefei Institutes of Physical Science, Chinese Academy of Sciences, Hefei, 230031, Anhui, China.*

[b] *Department of Chemistry, University of Science and Technology of China, Hefei, 230026, Anhui, China.*

‡ These authors contributed equally to this work.

**Corresponding Author**

* **Nian Li.** E-mail: linian@issp.ac.cn

* **Zhenyang Wang.** E-mail: zywang@iim.ac.cn

## Calculations of electrochemical performance:

1. The areal specific capacitance of EIG electrodes and EIG-MSC were calculated from galvanostatic charge/discharge (GCD) curves as follow equation:

$$C_A = \frac{I\Delta t}{A\Delta U} \tag{1}$$

where $C_A$ is the areal specific capacitance (mF $cm^{-2}$), $I$ is the discharge current (mA), $\Delta t$ is the discharge time (s), $\Delta U$ is the applied potential window (V), $A$ is the area of electrodes ($cm^2$).

2. The areal energy density ($E_A$, μWh·$cm^{-2}$), areal power density ($P_A$, mW·$cm^{-2}$), were calculated using the following equations, respectively:

$$E_A = \frac{1}{2} \times C_A \times \frac{(\Delta U)^2}{3600} \tag{2}$$

$$P_A = 3600 \times \frac{E_A}{\Delta t} \tag{3}$$

where $C_A$ is the areal specific capacitance (mF $cm^{-2}$), $\Delta U$ (V) is the potential window, and $\Delta t$ is the discharge time (s).

## Supporting Figures

a

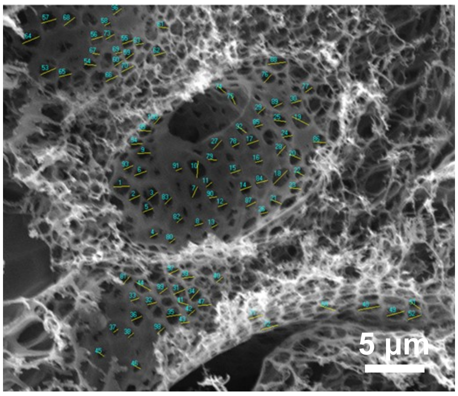


b

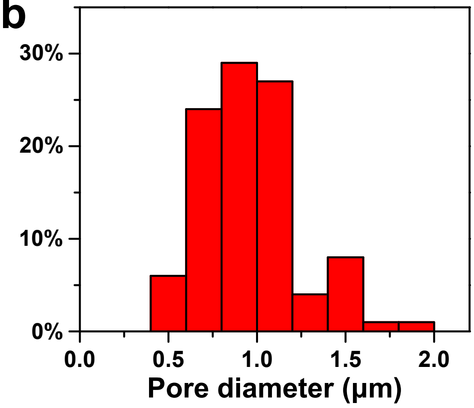


c

| Distribution (μm) | Average diameter (μm) | Accounts | Frequency |
|---|---|---|---|
| 0-0.2 | 0.1 | 0 | 0% |
| 0.2-0.4 | 0.3 | 0 | 0% |
| 0.4-0.6 | 0.5 | 6 | 6% |
| 0.6-0.8 | 0.7 | 24 | 24% |
| 0.8-1 | 0.9 | 29 | 29% |
| 1-1.2 | 1.1 | 27 | 27% |
| 1.2-1.4 | 1.3 | 4 | 4% |
| 1.4-1.6 | 1.5 | 8 | 8% |
| 1.6-1.8 | 1.7 | 1 | 1% |
| 1.8-2 | 1.9 | 1 | 1% |

**Fig. S1** (a) The selection of smaller holes on the pore wall of three-dimensional graphene network. (b) The histogram of pore diameter distribution. (c) Statistics of pore diameter.

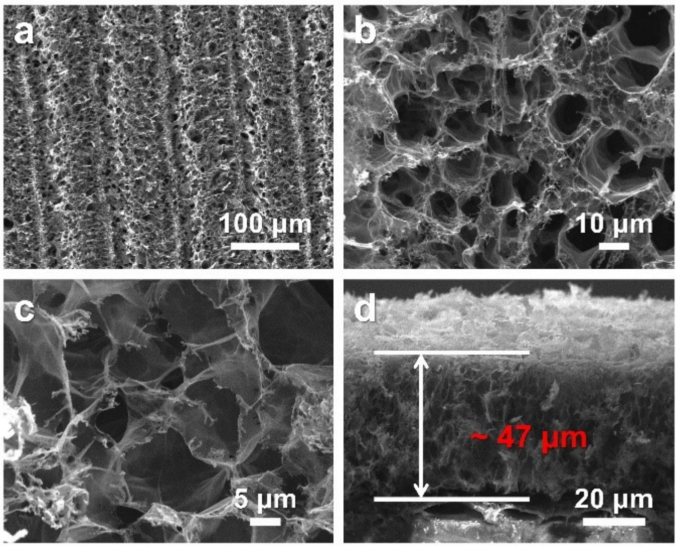


**Fig. S2** (a-c) The top view SEM images of LIG at different magnifications. (d) The corresponding cross-sectional SEM image of LIG.

**Supplementary note:**

Fig. S2 shows the SEM images of pure undoped LIG under different magnifications. Notably, different from N-LIG, there are few smaller pores on the pore wall of the graphene sheet network in LIG.

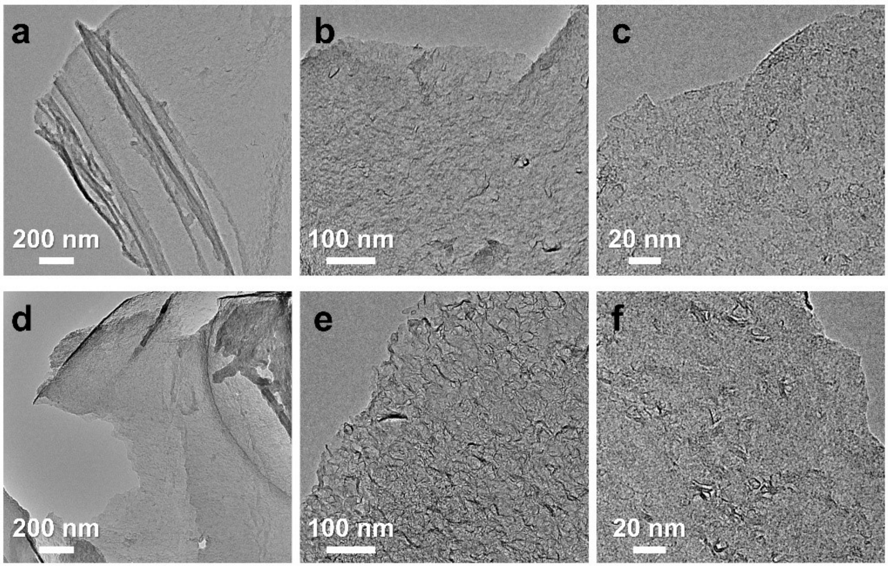


**Fig. S3** TEM images of (a-c) LIG, and (d-f) N-LIG.

**Supplementary note:**

Fig. S3 reveals the TEM images of LIG and N-LIG. It can be seen that both LIG and N-LIG possess the thin layer morphology.

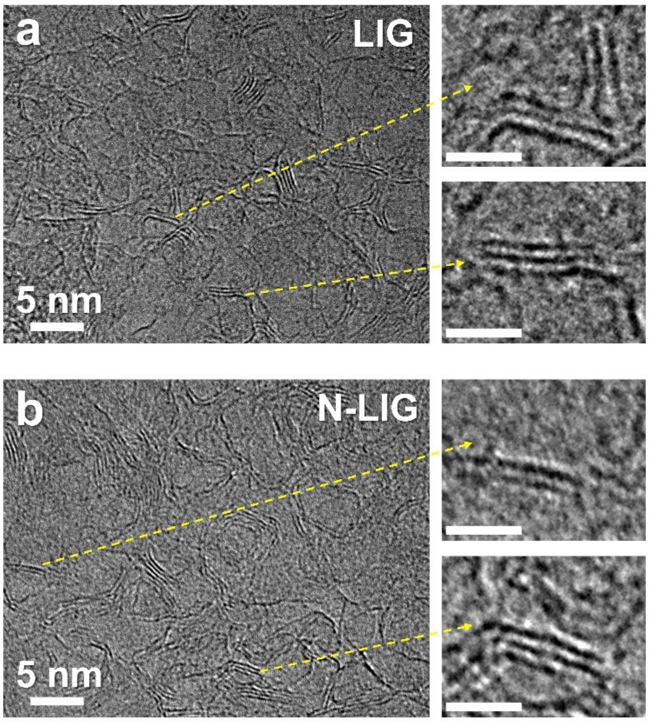


**Fig. S4** HRTEM images of (a) LIG, and (b) N-LIG. The scale bars of insets are 2 nm.

**Supplementary note:**

As shown in HRTEM images (Fig. S4), there is no distinct difference in the number of carbon layers between LIG and N-LIG. The insets of Fig. S4 show the small number of local interlayer wrinkles of graphene, proving that both of them possess few-layer structure (such as 3 layers).

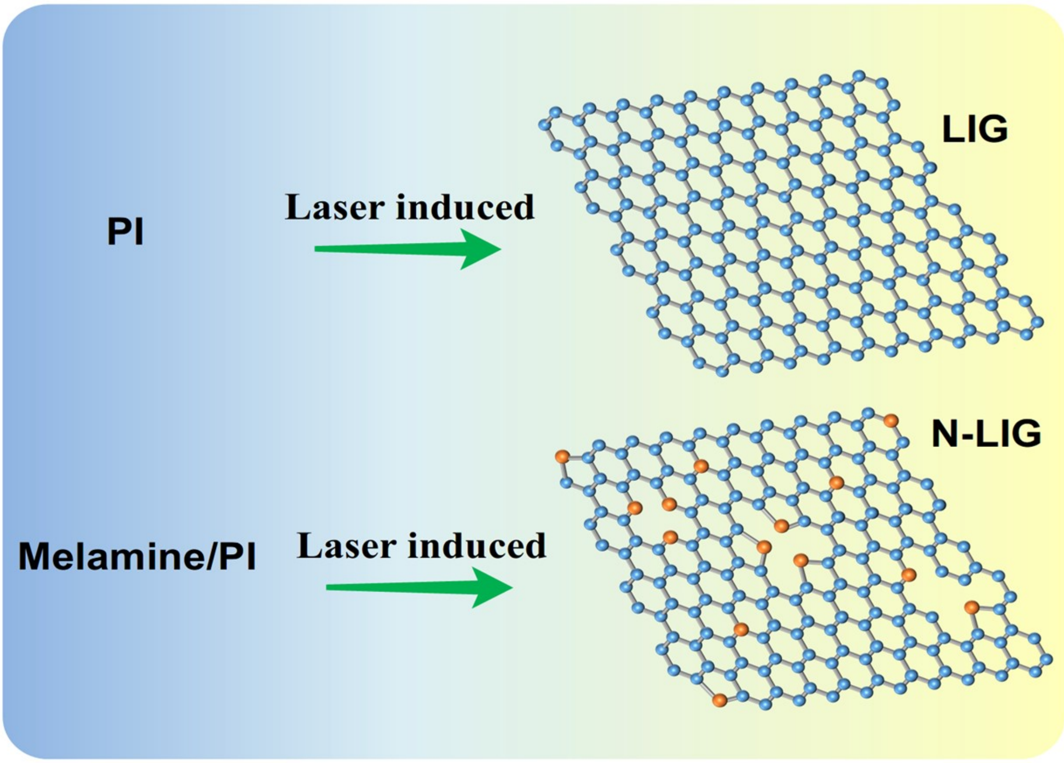


**Fig. S5** Schematic diagram of the preparation and structure of laser-induced graphite (LIG) and nitrogen-doped laser-induced graphene (N-LIG).

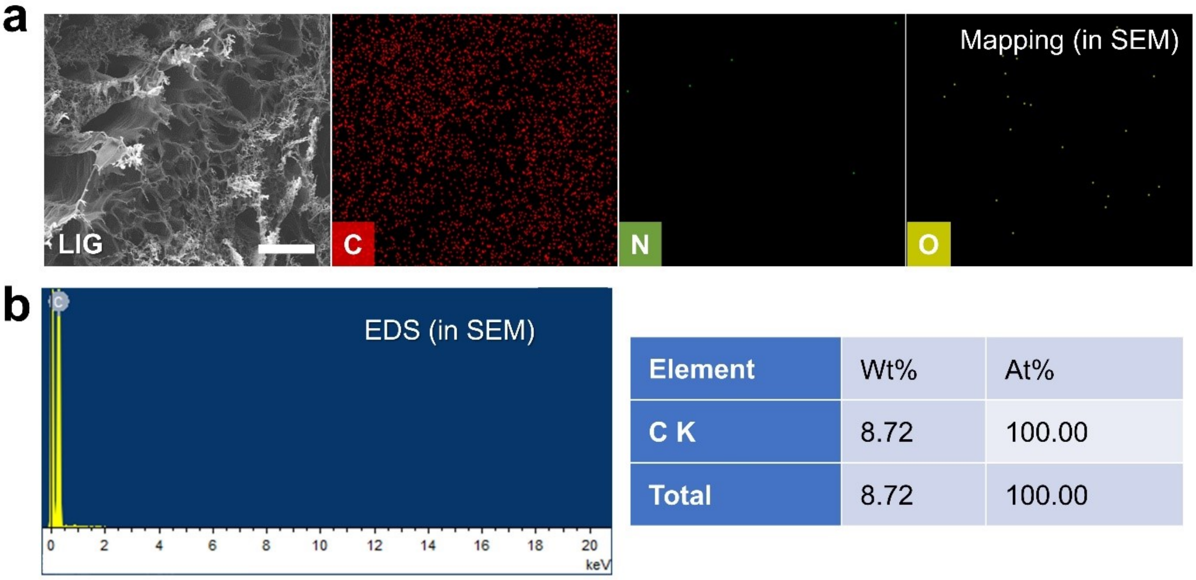


| Element | Wt% | At% |
|---|---|---|
| C K | 8.72 | 100.00 |
| Total | 8.72 | 100.00 |

**Fig. S6** (a) The elemental mapping results and (b) EDS spectrum in SEM of LIG sample. (The scale bar in the figure is 20 μm).

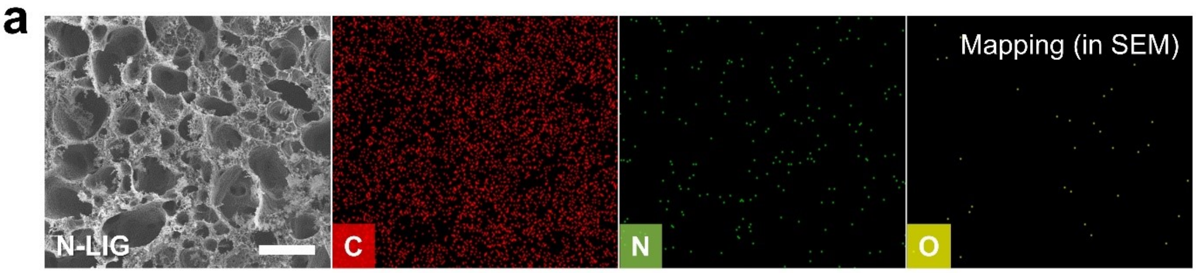


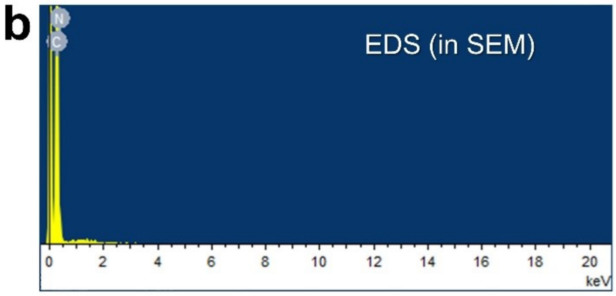


| Element | Wt% | At% |
|---|---|---|
| C K | 8.23 | 88.89 |
| N K | 1.20 | 11.11 |
| Total | 9.43 | 100.00 |

**Fig. S7** (a) The elemental mapping results and (b) EDS spectrum in SEM of N-LIG sample. (The scale bar in the figure is 20 μm).

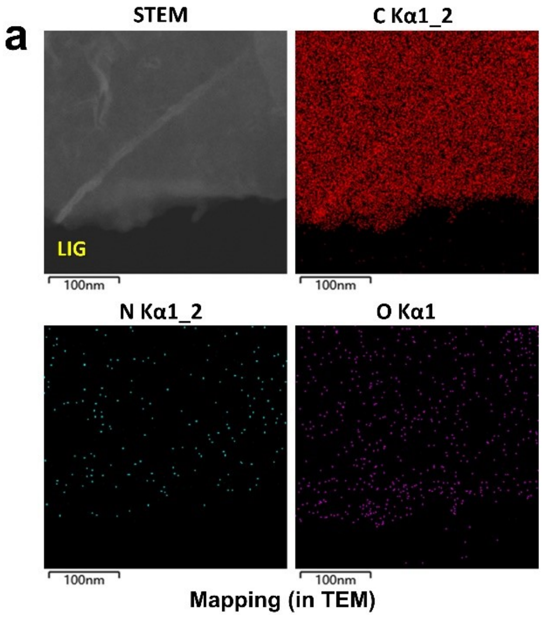


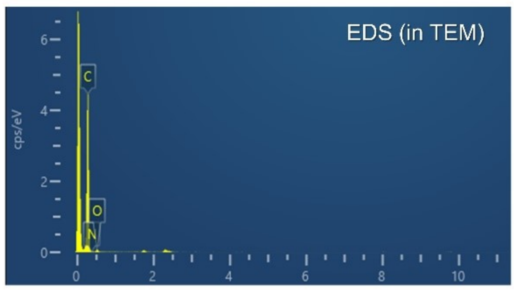


| element | wt% | wt% sigma | at% |
|---|---|---|---|
| C K | 99.13 | 0.08 | 99.35 |
| N K | 0.00 | 0.00 | 0.00 |
| O K | 0.87 | 0.08 | 0.65 |
| Total | 100.00 | | 100.00 |

**Fig. S8** (a) The elemental mapping results and (b) EDS spectrum in TEM of LIG sample.

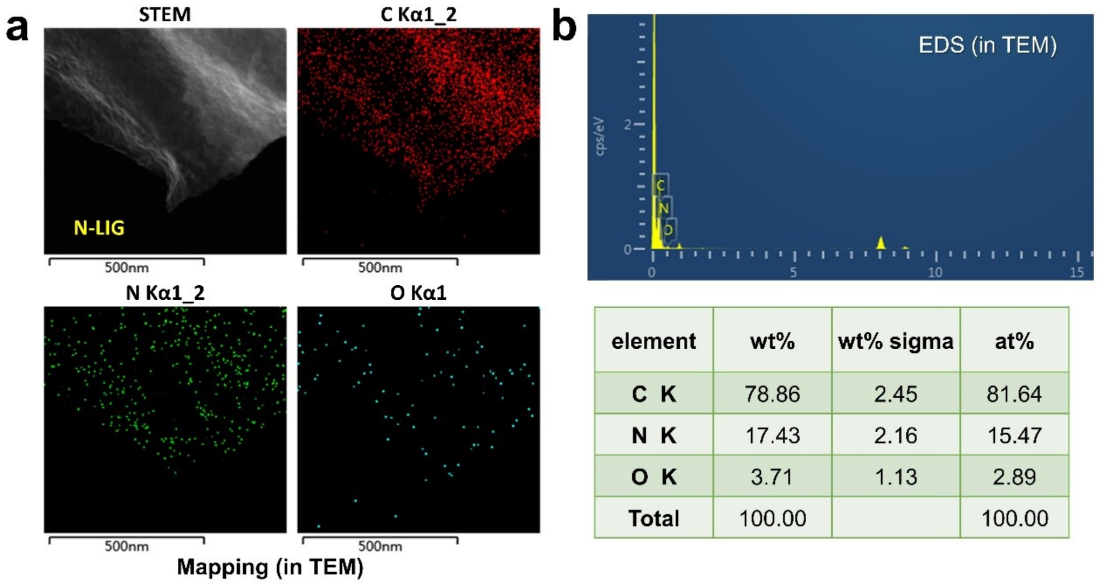


| element | wt% | wt% sigma | at% |
| --- | --- | --- | --- |
| C K | 78.86 | 2.45 | 81.64 |
| N K | 17.43 | 2.16 | 15.47 |
| O K | 3.71 | 1.13 | 2.89 |
| Total | 100.00 | | 100.00 |

**Fig. S9** (a) The elemental mapping results and (b) EDS spectrum in TEM of N-LIG sample.

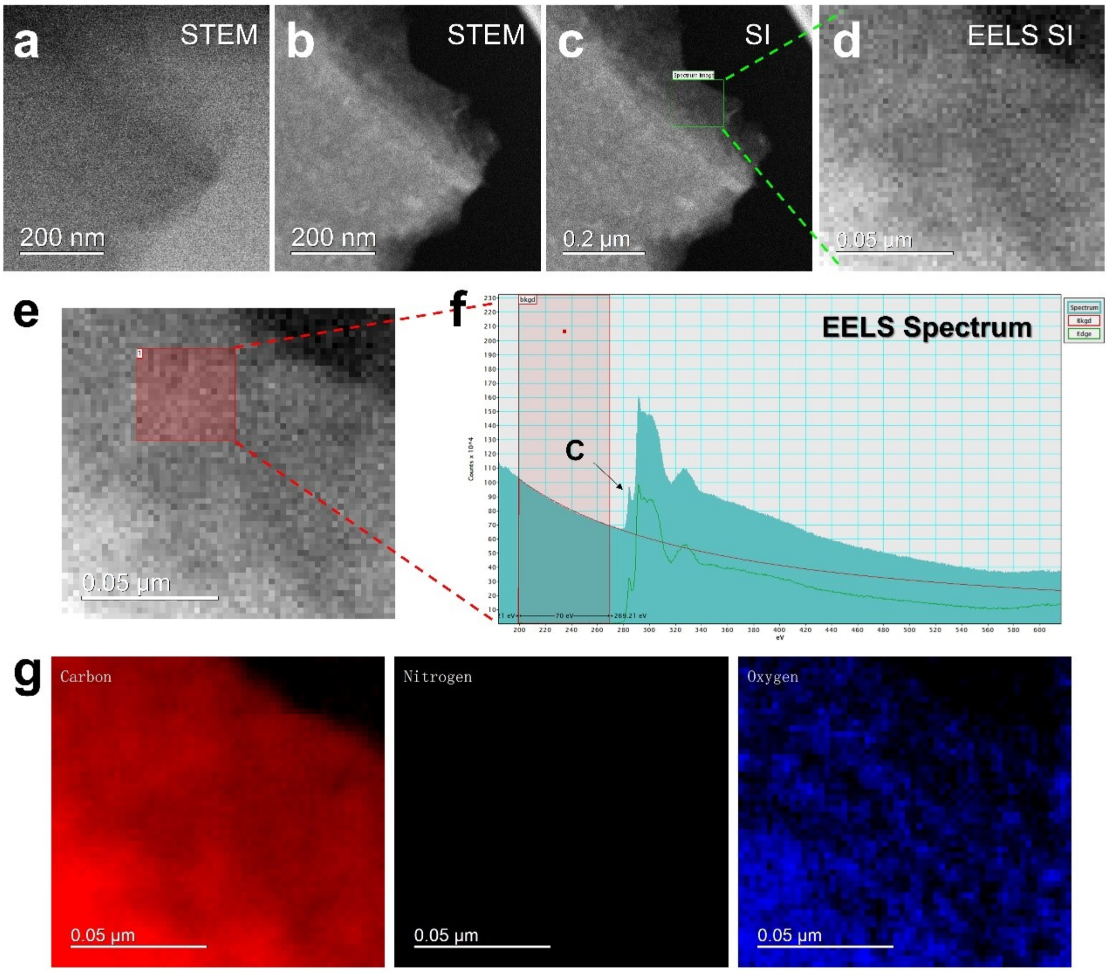


**Fig. S10** (a-b) The STEM images of LIG. (c) Location of EELS spectrum image (SI). (d) EELS SI of LIG. (e-f) Specifical EELS spectrum of LIG. (g) Elemental distribution of LIG in EELS SI.

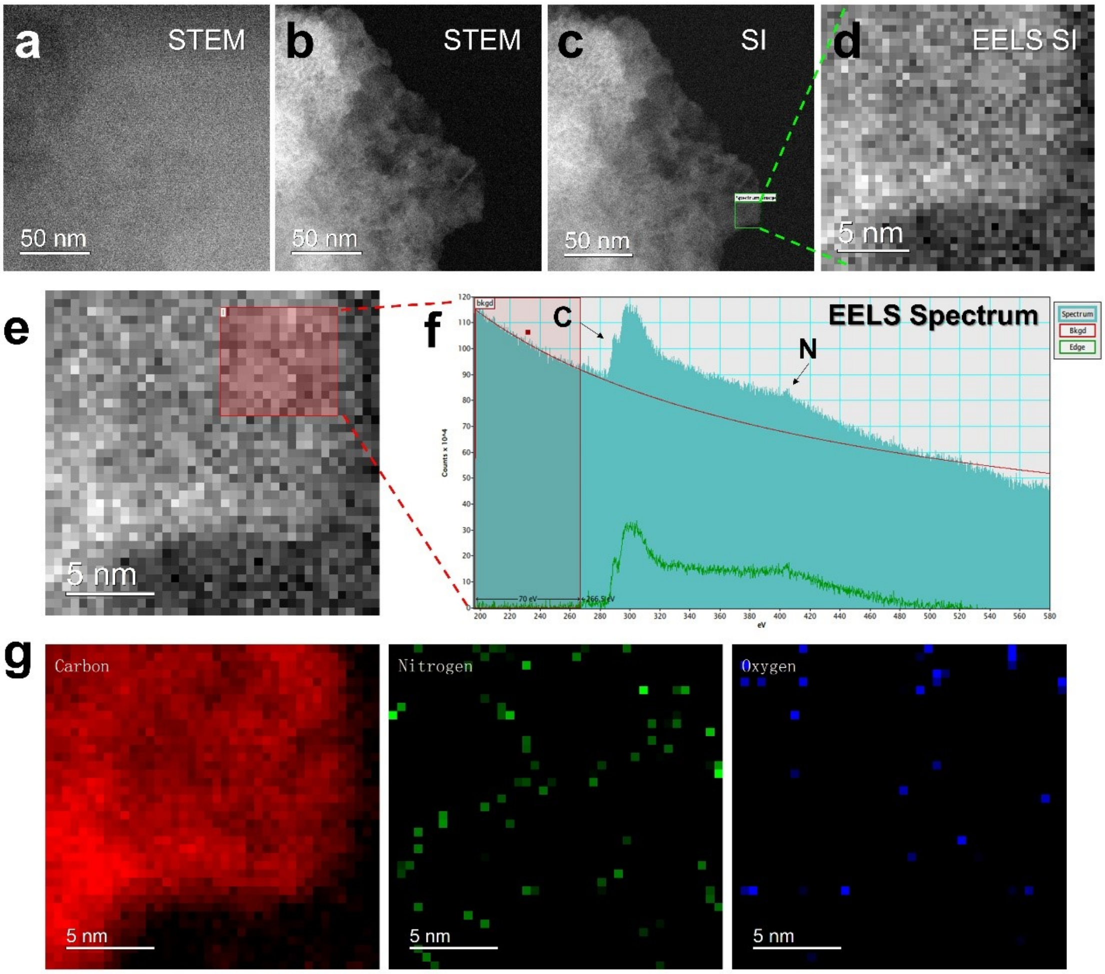


**Fig. S11** (a-b) The STEM images of N-LIG. (c) Location of EELS spectrum image (SI). (d) EELS SI of N-LIG. (e-f) Specifical EELS spectrum of N-LIG. (g) Elemental distribution of N-LIG in EELS SI.

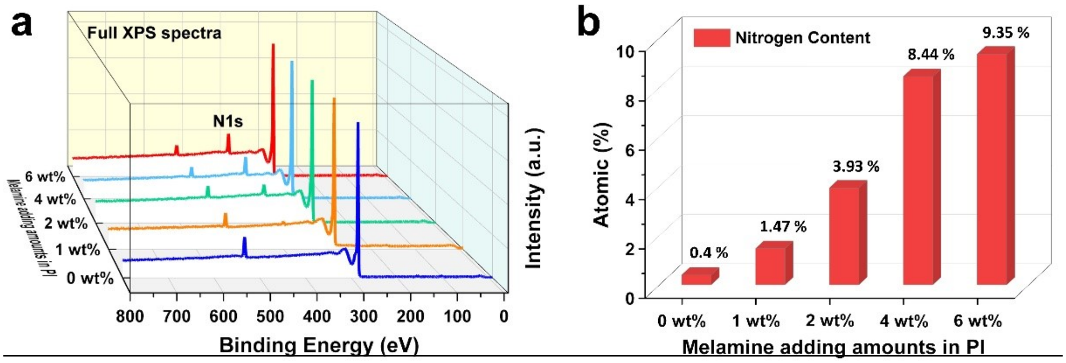


**Fig. S12** (a) XPS spectra of different LIG and N-LIG samples obtained from composite films with different melamine-adding amounts in PI. (b) The corresponding atomic proportion of nitrogen of different samples.

**Supplementary note:**

Fig. S12 shows the XPS spectra and nitrogen atomic proportion of different LIG and N-LIG samples. In Fig. S12a, it can be seen that the N1s peaks of different as-prepared N-LIG samples are gradually enhanced with the increase of the melamine-adding amounts (0 wt%, 1 wt%, 2 wt%, 4 wt%, 6 wt%) in PI. Moreover, as shown in Fig. S12b, the atomic proportion of nitrogen in N-LIG gradually increases correspondingly (N atomic: 0.4%, 1.47%, 3.93%, 8.44%, 9.35%). Remarkably, when the melamine-adding amounts in PI increases from 4 wt% to 6 wt%, the increasing extent of nitrogen content in the obtained samples slowed down (only from 8.44% to 9.35%).

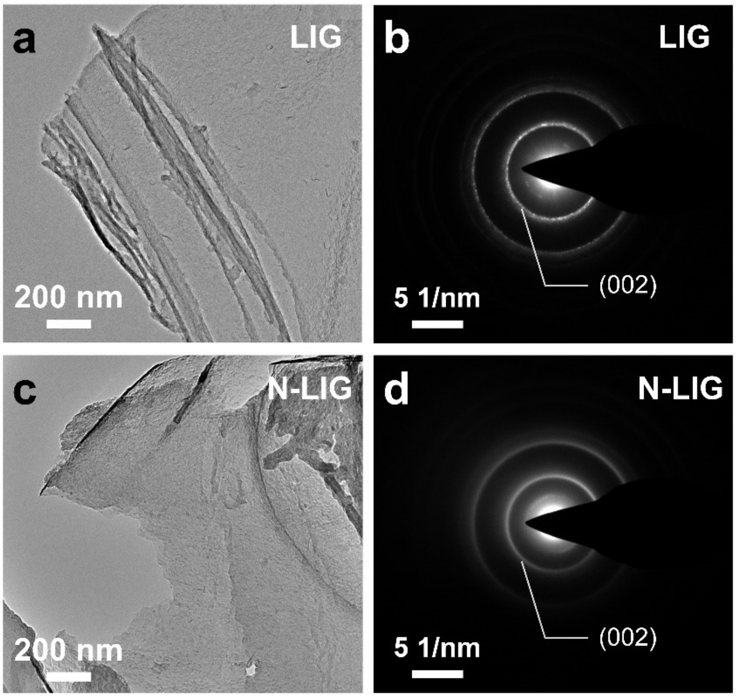


**Fig. S13** SAED results of (a-b) LIG, and (c-d) N-LIG.

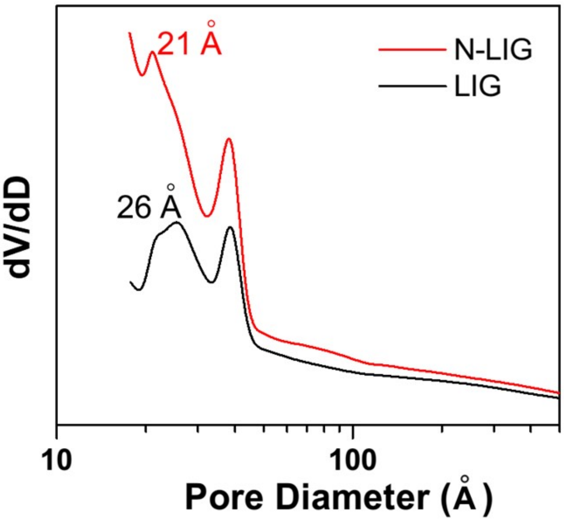


**Fig. S14** Pore distribution of laser-induced graphite (LIG) and nitrogen-doped laser-induced graphene (N-LIG).

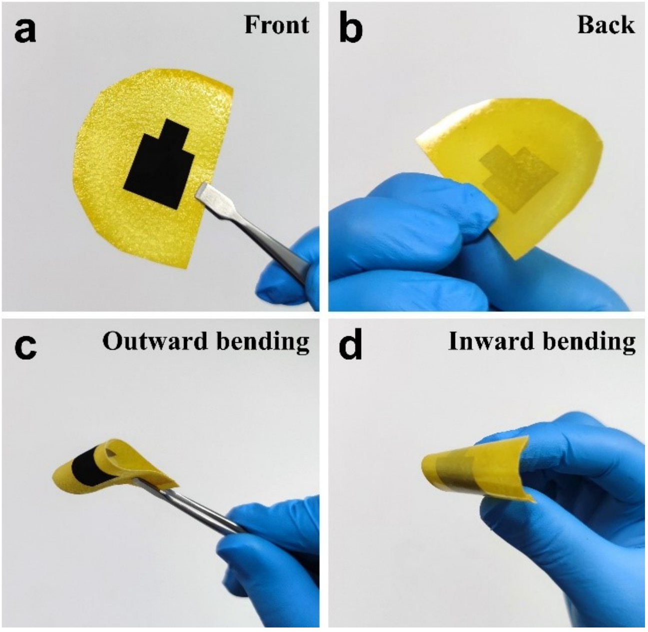


**Fig. S15** The digital photos of the flexible N-LIG electrode obtained on melamine/polyimide film with 6 wt% compounding amounts of melamine.

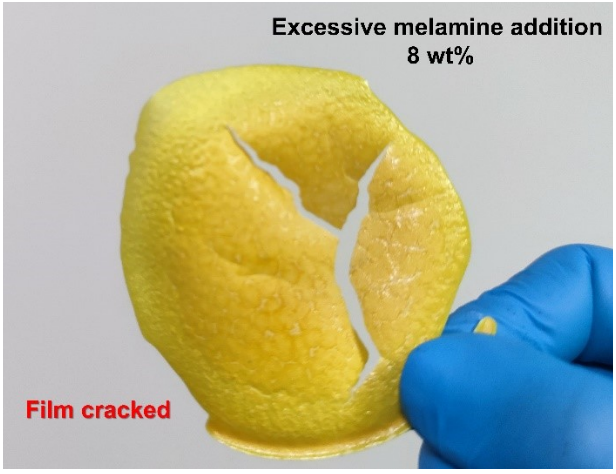


**Fig. S16** The digital photo of the melamine/polyimide composite film with 8 wt% compounding amounts of melamine.

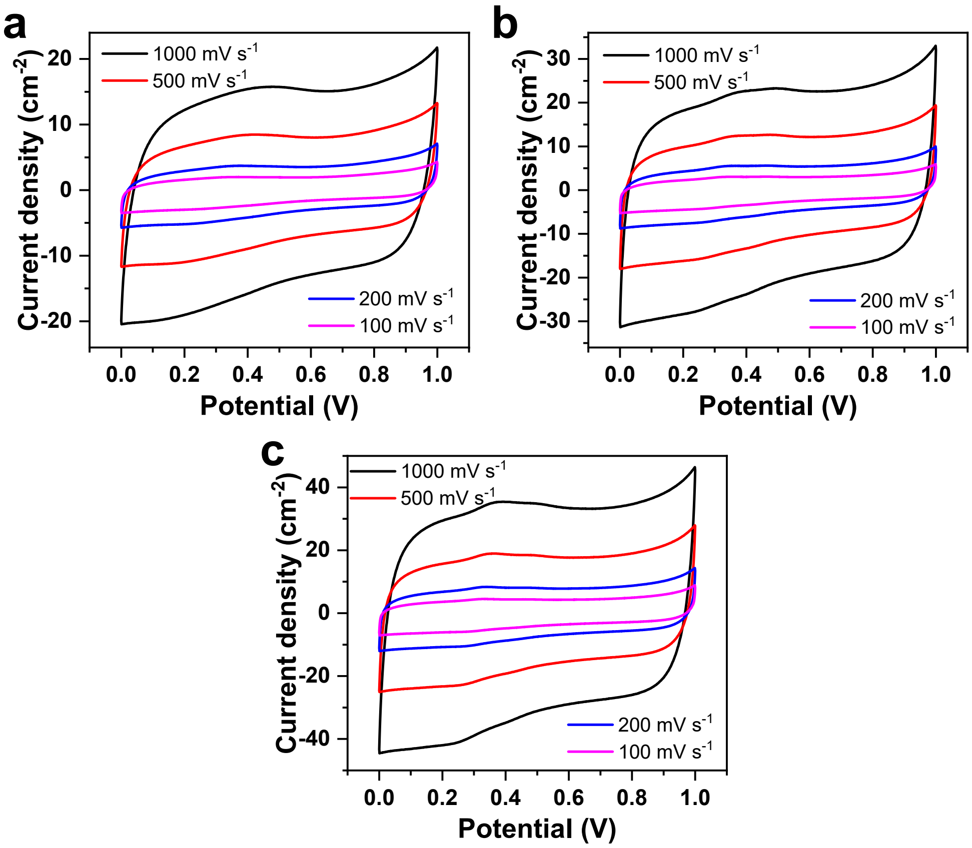


**Fig. S17** The CV curves of N-LIG electrode prepared by melamine/polyimide composite film with melamine compounding amounts (a-c, 1 wt%, 2 wt%, 4 wt%).

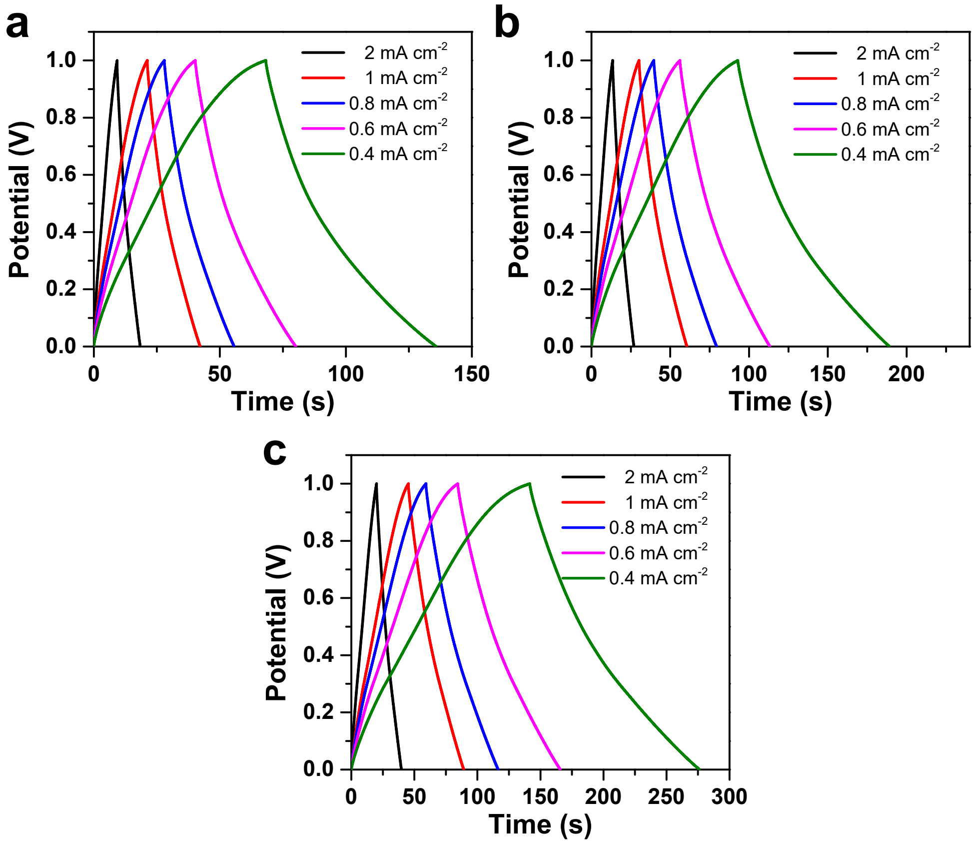


**Fig. S18** The GCD plots of N-LIG electrode prepared by melamine/polyimide composite film with melamine compounding amounts (a-c, 1 wt%, 2 wt%, 4 wt%).

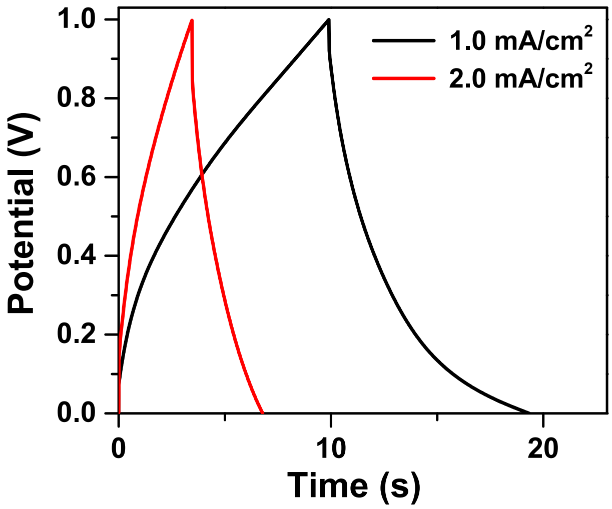


**Fig. S19** GCD plots of N-LIG MSC at high current densities of 1.0 and 2.0 mA $cm^{-2}$.

## Supporting Table

**Table S1.** A comparison of capacitive performance of N-LIG MSC fabricated in the present work with other graphene-based MSCs.

| MSC material | Method | Electrolyte | Condition | $C_A$ (mF/cm$^2$) | Energy density (μWh/cm$^2$) | Ref. |
|---|---|---|---|---|---|---|
| **N-LIG** | **Laser induction** | **PVA/$H_2SO_4$** | **0.05 mA cm$^{-2}$** | **35.20** | **4.89** | **This work** |
| LIG | Laser induction | PVA/$H_2SO_4$ | 0.02 mA cm$^{-2}$ | $>$9.00 | 1.25 | [1] |
| s-LIG | Laser induction | PVA/$H_2SO_4$ | 0.05 mA cm$^{-2}$ | 5.00 | 0.69 | [2] |
| Fs-LIG | Laser induction | PVA/$H_2SO_4$ | 0.10 mA cm$^{-2}$ | 22.40 | 3.11 | [3] |
| Air-plasma treated LIG | Laser induction | PVA/$H_2SO_4$ | 0.02 mA cm$^{-2}$ | 28.50 | 3.96 | [4] |
| Lignin/PVA-based LIG | Laser induction | PVA/$H_2SO_4$ | 0.05 mA cm$^{-2}$ | 25.10 | 3.49 | [5] |
| SPEEK-based LIG | Laser induction | 1 M $Na_2SO_4$ | 0.20 mA cm$^{-2}$ | 1.90 | 0.39 | [6] |
| LIAG/KC-35 | Laser induction | PVA/$H_3PO_4$ | 0.05 mA cm$^{-2}$ | 30.06 | 4.01 | [7] |
| N-d-LIG | Laser induction | PVA/$H_2SO_4$ | 0.05 mA cm$^{-2}$ | 20.80 | 2.89 | [8] |
| B-LIG | Laser induction | PVA/$H_2SO_4$ | 0.05 mA cm$^{-2}$ | 16.50 | 2.29 | [9] |
| N-doped LIG with PEDOT | Laser induction | PAAK/KOH | 0.05 mA cm$^{-2}$ | 0.79 | 0.07 | [10] |
| $MoS_2$-LIG | Laser induction | PVA/$H_2SO_4$ | 0.10 mA cm$^{-2}$ | 16.20 | 2.25 | [11] |
| N-doped rGO | Screen printing | PVA/$H_3PO_4$ | 0.02 mA cm$^{-2}$ | 3.40 | 0.30 | [12] |

## References


1. Z. Peng, J. Lin, R. Ye, E. L. G. Samuel and J. M. Tour, *ACS Applied Materials & Interfaces*, 2015, **7**, 3414-3419.
2. K. Y. Kim, H. Choi, C. V. Tran and J. B. In, *Journal of Power Sources*, 2019, **441**, 227199.
3. S. Wang, Y. Yu, R. Li, G. Feng, Z. Wu, G. Compagnini, A. Gulino, Z. Feng and A. Hu, *Electrochimica Acta*, 2017, **241**, 153-161.
4. J. Cai, C. Lv and A. Watanabe, *Nano Energy*, 2016, **30**, 790-800.
5. W. Zhang, Y. Lei, F. Ming, Q. Jiang, P. M. F. J. Costa and H. N. Alshareef, *Advanced Energy Materials*, 2018, **8**, 1801840.
6. A. Lamberti, M. Serrapede, G. Ferraro, M. Fontana, F. Perrucci, S. Bianco, A. Chiolerio and S. Bocchini, *2D Materials*, 2017, **4**, 035012.
7. H. Liu, Y. Xie, J. Liu, K.-s. Moon, L. Lu, Z. Lin, W. Yuan, C. Shen, X. Zang, L. Lin, Y. Tang and C.-P. Wong, *Chemical Engineering Journal*, 2020, **393**, 124672.
8. M. Khandelwal, C. V. Tran, J. Lee and J. B. In, *Chemical Engineering Journal*, 2022, **428**, 131119.
9. Z. Peng, R. Ye, J. A. Mann, D. Zakhidov, Y. Li, P. R. Smalley, J. Lin and J. M. Tour, *ACS Nano*, 2015, **9**, 5868-5875.
10. W. Song, J. Zhu, B. Gan, S. Zhao, H. Wang, C. Li and J. Wang, *Small*, 2018, **14**, 1702249.
11. S. Wang, Y. Yu, S. Luo, X. Cheng, G. Feng, Y. Zhang, Z. Wu, G. Compagnini, J. Pooran and A. Hu, *Applied Physics Letters*, 2019, **115**, 083904.
12. S. Liu, J. Xie, H. Li, Y. Wang, H. Y. Yang, T. Zhu, S. Zhang, G. Cao and X. Zhao, *Journal of Materials Chemistry A*, 2014, **2**, 18125-18131.